

# SYNTHESIS, CHARACTERIZATION AND SURFACE DEFORMATION STUDY OF NANOCRYSTALLINE Ag<sub>2</sub>Se THIN FILMS

U.M. Chougale<sup>1</sup>, S.H. Han<sup>2</sup>, M.C. Rath<sup>3</sup>, V.J. Fulari<sup>1\*</sup>

<sup>1</sup>Holography and Materials Research Laboratory, Department of Physics, Shivaji University,  
Kolhapur-416 004, India

<sup>2</sup>Department of Chemistry, Hanyang University, Seoul, South Korea.

<sup>3</sup>Radiation and Photochemistry Division, BARC, Mumbai, India

\*e-mail: vijayfulari@gmail.com

**Abstract.** Herein we report electrochemical synthesis of the silver selenide (Ag<sub>2</sub>Se) thin films using simple and economical electrodeposition method in potentiostatic mode at room temperature (~ 27 °C). Growth of rhombohedral Ag<sub>2</sub>Se nanocrystals having size 63 to 75 nm were observed in (201) direction. Band gap energy of Ag<sub>2</sub>Se decreased from 1.3 eV to 1.1 eV and contact angle increases from 58 ° to 74 ° with increase in bath concentration from 3 to 5 mM. A possible mechanism for the growth and stress of compact granular Ag<sub>2</sub>Se nanocrystals is discussed with DEHI technique. Compared with previous methods, present method shows simple and easiest way to synthesize nanosized Ag<sub>2</sub>Se particles in one step.

## 1. Introduction

Silver selenide (Ag<sub>2</sub>Se) belongs to I–VI semiconductor compound rarely found in the nature as mineral naumannite. Silver selenide (Ag<sub>2</sub>Se) is a promising material for technological applications in various fields such as thermo-chromic material for non-linear optical devices, multipurpose ion-selective electrodes, infrared sensors, electrochemical storage cells, electrochemical potential memory devices, magnetic field sensing devices etc [1-3]. Silver selenide ( $\beta$ - Ag<sub>2</sub>Se) is an important n-type semiconductor with a narrow band gap [4, 5]. Ag<sub>2</sub>Se is a mixed ionic conductor with a transition from a low temperature orthorhombic phase ( $\beta$ - Ag<sub>2</sub>Se) to a high-temperature super ionic conducting cubic phase ( $\alpha$ - Ag<sub>2</sub>Se) at 135 °C [6]. Its high temperature phase ( $\alpha$ -Ag<sub>2</sub>Se) is a super-ionic conductor used as solid electrolyte in photochargable batteries [7]. Its low temperature phase ( $\beta$ -Ag<sub>2</sub>Se) has been widely exploited as a thermo-chromic material, as photo sensitizer in photographic films [8]. Nonstoichiometric Ag<sub>2</sub>Se also shows giant magneto resistance comparable to the colossal magneto resistance observed in manganese perovskites [9, 10]. All the above properties of Ag<sub>2</sub>Se are studied in bulk form and the physical properties of semiconducting material are size dependent. As semiconductor nanocrystals finding various applications in solar cells [11], light-emitting diodes [12, 13], thin-film transistors [14, 15] and biological imaging [16], the control over particle size and morphology became very much important from a fundamental and industrial point of view. In this direction synthesis of Ag<sub>2</sub>Se with different methods has been carried out by various workers. Vacuum evaporated Ag<sub>2</sub>Se thin films were used to study the phase transition temperature as a function of thickness [17]. Substitution deposition method [18], adsorption- reduction method [19], chemical bath deposition [20], reactive evaporation method [5], electrodeposition [21, 22] and solvo-thermal technique [23]

have been reported.

Variety of synthesis methods causes inconsistency in the properties of  $\text{Ag}_2\text{Se}$ . In this context very few workers have been reported on electrodeposited silver selenide from aqueous solution. Also high quality  $\text{Ag}_2\text{Se}$  nanocrystals could improve the performance in applications by changing its parameters such as size or crystal phase [24]. Motivated by this we are reporting here the effect of precursor concentration on the electro synthesis of nano crystalline  $\text{Ag}_2\text{Se}$  thin films at room temperature from aqueous electrolyte. For the nano structured materials most of the physical properties are depending upon the crystallographic structure and arrangement of atoms due to high surface to volume ratio, the main emphasis is on the effect of precursor concentration on the synthesis and physical properties of nanocrystalline  $\text{Ag}_2\text{Se}$  thin films are explained with double exposure holographic interferometry (DEHI) as a non destructive analytical tool.

## 2. Experimental

**2.1. Chemicals.** Silver nitrate ( $\text{AgNO}_3$ ) was obtained from s d Fine Chem. Ltd., Selenium dioxide ( $\text{SeO}_2$ ) was obtained from Thomas baker chemicals, Mumbai while Ethylene diamine tetra acetic acid (EDTA) was purchased from Himedia chemicals Ltd., Mumbai. All chemicals were high grade reagents and were used as received without further purification. Double distilled de-ionized water was used as solvent for precursor solution.

**2.2. Electrolyte bath preparation.** First the precursors  $\text{AgNO}_3$ ,  $\text{SeO}_2$  and EDTA were dissolved in double distilled water separately with different molar concentrations for each viz 0.03, 0.04 and 0.05 M. The electrolyte baths (A), (B) and (C) for  $\text{Ag}_2\text{Se}$  thin film depositions contain 0.03, 0.04 and 0.05 M of  $\text{AgNO}_3$ ,  $\text{SeO}_2$ , and EDTA in 1:1:1 ratio respectively. pH value was maintained  $\sim 3$ . The electrodeposition of  $\text{Ag}_2\text{Se}$  was carried out at 300 °K using a potentiostat (Princeton PerkinElmer, Applied Research Versastat-II; Model 250/270) with three electrode configuration in which Saturated calomel electrode (SCE,  $E = 0.241 \text{ V/SHE}$ ) was used as reference electrode. Stainless steel (304) substrates of dimensions  $5 \times 1 \times 0.03 \text{ cm}^3$  and FTO doped glass substrates were used as the working electrode while graphite of dimension  $5 \times 1 \times 0.5 \text{ cm}^3$  was used as counter electrode. Potentials were measured and reported versus SCE. Prior to electrodeposition, the stainless steel substrates were polished by zero grade polish paper and cleaned by acetone first and then with double distilled water in ultrasonic cleaner for 15 minutes. Further the substrates were rinsed with double distilled water and then dried.

**2.3. Instrumentation.** The structural determination was carried out by a Philips PW-1710 X-ray diffractometer with a Cr  $K\alpha$  ( $\lambda = 2.2870 \text{ \AA}$ ) target. Scanning Electron Microscope (JEOLJSM-6360) was used for morphological study. Optical absorption in the wavelength range of 350-800 nm was studied using UV-VIS spectrometer (Hitachi model-3600). The contact angle meter (Rame hart, model 500-F1, USA) was used to determine surface wettability of the films. FT-IR spectra were recorded on a spectrophotometer (Perkin Elmer FT-IR Spectrum-GX), at laser power 0-450 mW and wave number range from 500-4000  $\text{cm}^{-1}$ .

## 3. Results and discussion

**3.1. Synthesis.** Cyclic voltammetry is used to determine the formal potential of half reaction as an identification tool for stable both oxidized and reduced forms. The potential of the working electrode is measured against a reference electrode which maintains a constant potential and the resulting applied potential produces an excitation signal [25]. The reduction potentials of Ag, Se,  $\text{Ag}_2\text{Se}$  compound are found by the cyclic voltammograms recorded on stainless steel substrate from 5 mM electrolytic solutions of  $\text{AgNO}_3$ ,  $\text{SeO}_2$  and ( $\text{AgNO}_3 + \text{EDTA} + \text{SeO}_2$ ) respectively. Figure 1 (a-c) shows electrochemical behavior of the solutions due to applied potential. The reduction peak at -0.5 to -0.8 V is associated with formation of

Ag (Fig. 1(a)), while reduction of  $\text{Se}^{4+}$  to Se occurs at -0.1 to -0.45 V (Fig. 1(b)). There are two anodic peaks on curve corresponding to the oxidation of Ag (at 0.8 V) and oxidation of  $\text{Se}^{2-}$  to  $\text{Se}^0$  (at -0.45 V) (Fig. 1(c)).  $\text{Se}^{2-}$  is formed during the reduction of  $\text{H}_2\text{SeO}_3$  (at -0.1 V). Oxidation of Se to  $\text{Se}^{4+}$  occurs at -1.0 V. Cathodic peak at -0.7 V is related with reduction of  $\text{Se}^{4+}$  to Se while reduction of  $\text{Ag}^+$  occurs at +0.4 V [26]. From Fig. 1(c) it is seen that the cathodic current increases -0.2 V to -0.4 V. Thus the deposition of  $\text{Ag}_2\text{Se}$  takes place at this particular reduction potential [27].

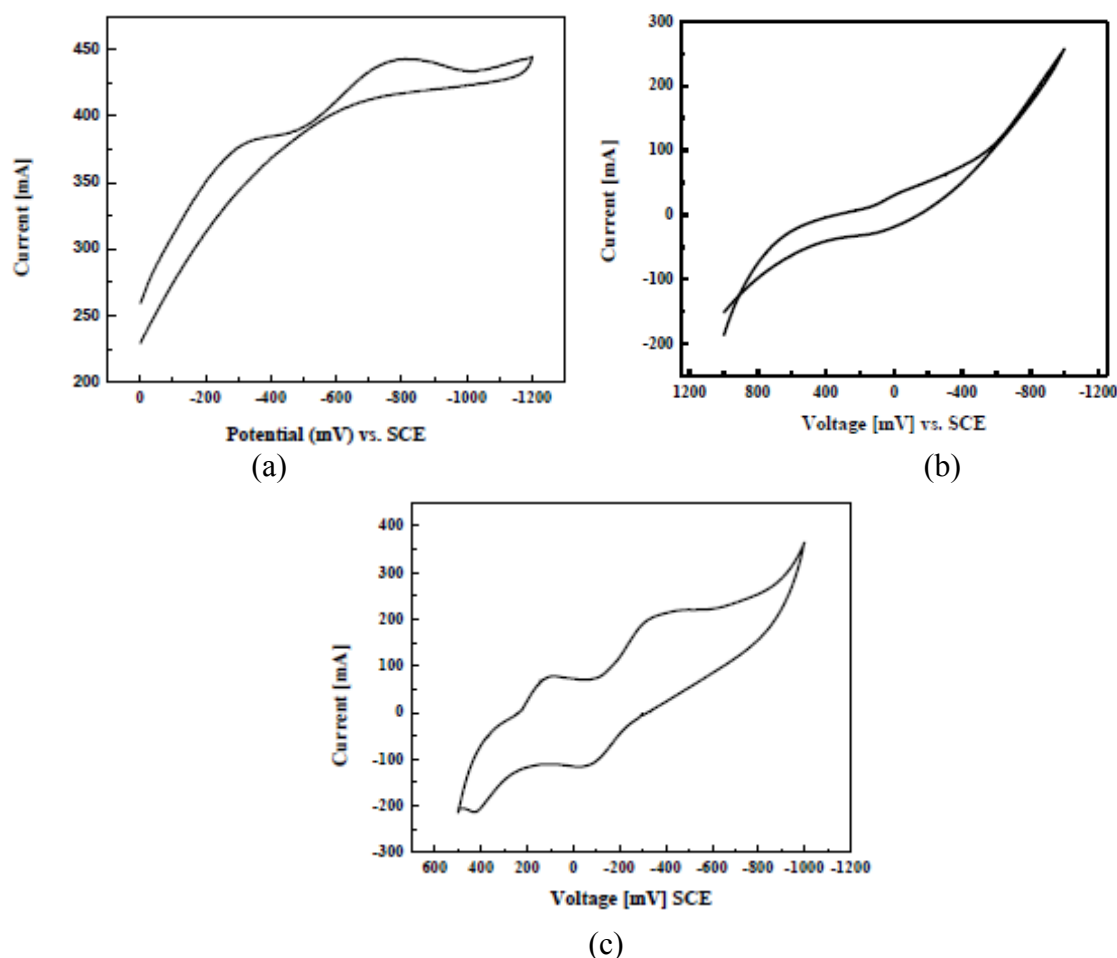


**Fig. 1.** Cyclic voltammogram for (a) 5 mM  $\text{AgNO}_3$ , (b) 5 mM  $\text{SeO}_2$ , (c) 5 mM ( $\text{AgNO}_3 + \text{SeO}_2$ ).

**3.2. Reaction mechanism.** The chemical reaction for the deposition of silver selenide films taking place in bath could be considered as below:

The aqueous solution of silver nitrate forms



Selenium dioxide forms



The final reaction takes place for the formation of  $\text{Ag}_2\text{Se}$  film:



**3.3. X-ray diffraction.** Figure 2 shows X-ray diffraction patterns of three  $\text{Ag}_2\text{Se}$  thin film samples I, II and III for different bath concentration (A), (B) and (C) respectively

deposited on stainless steel substrate for same deposition time of 15 min.

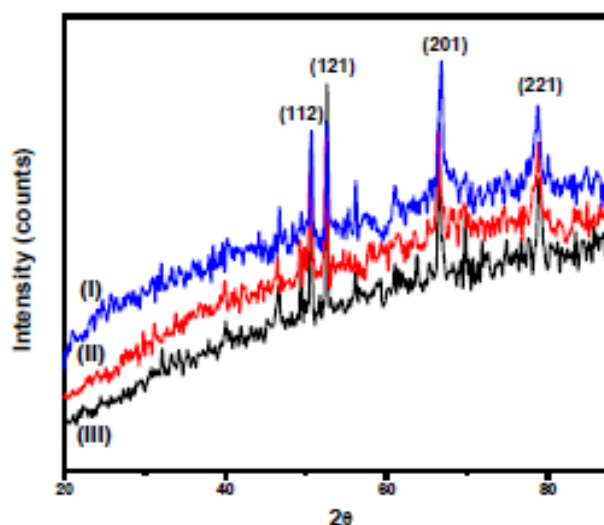


Fig. 2. X-ray diffraction patterns of Ag<sub>2</sub>Se thin films.

These diffraction patterns are formed by the x-rays obeying Bragg's law:

$$n\lambda = 2d \sin\theta, \quad (3)$$

where all symbols have their usual meaning [28]. All of the samples shows similar XRD pattern. Some peaks observed for bath concentration (A) are not observed for (B) and (C). It means, growth of the film in those directions is suppressed and is persistent in particular directions. The observed „d“ values are in good agreement with standard values [29] arranged in Table 1.

Table 1. Comparison of observed and standard „d“ values of Ag<sub>2</sub>Se.

Sr. No	Observed 'd', Å	Standard 'd', Å	(hkl) plane
01	2.6752	2.6730	(112)
02	2.5812	2.5810	(121)
03	2.0797	2.0800	(201)
04	1.7980	1.7960	(221)

Ag<sub>2</sub>Se thin films have low temperature orthorhombic ( $\beta$ -Ag<sub>2</sub>Se) crystal structure with lattice constants of  $a = 4.3330 \text{ \AA}$ ,  $b = 7.0620 \text{ \AA}$ ,  $c = 7.7640 \text{ \AA}$  and  $\alpha = \beta = \gamma = 90^\circ$ . Dominant plane (201) was used to calculate the particle size of Ag<sub>2</sub>Se film with the help of Scherer's formula [30]:

$$D = 0.9\lambda / \beta \cos\theta. \quad (4)$$

As the bath concentration increases from 3 to 5mM, the crystallite size also increases from 63.41 nm to 75.22 nm. Increase in particle size for different orientations of crystallographic planes is summarized in table no. 2. The crystal growth takes place in (201) direction prominently. The enhancement of particle size with increase in concentration is related to the nucleation and growth mechanism in thin film.

Table 2. Variation in particle size, contact angle and band gap energy of  $\text{Ag}_2\text{Se}$  thin films.

Sample	Particle size for (hkl) planes, nm			Contact Angle, degree		Band gap energy, eV	
	(112)	(121)	(201)	(221)	Mean		
A	55.90	62.45	62.40	72.88	63.41	58	1.31
B	56.40	66.27	66.46	86.05	68.80	63	1.20
C	90.19	62.46	62.40	85.83	75.22	74	1.13

**3.4. Surface morphology.** The microstructure of  $\text{Ag}_2\text{Se}$  thin films on to stainless steel substrate was analyzed by scanning electron microscope technique for samples I, II and III. From the micrographs (Fig. 3), it is seen that the  $\text{Ag}_2\text{Se}$  particles cluster into uniformly distributed grains over smooth homogenous background. Also grain size increases with increasing concentration. The growth of the nanostructures takes place through two steps namely nucleation followed by growth, in first step the  $\text{Ag}_2\text{Se}$  nuclei are formed due to the applied potential. These nuclei having high surface energy tend to aggregate by minimizing interfacial energy which tends to larger particle size. This suggests that increase in bath concentration favor both particle growth and aggregation. The well developed and matured  $\text{Ag}_2\text{Se}$  particle growth is observed as Van der Waals interaction between  $\text{Ag}_2\text{Se}$  leads to the self assembly and aggregation of  $\text{Ag}_2\text{Se}$  nanocrystals [31]. Different methods yield different morphologies of  $\text{Ag}_2\text{Se}$  thin films used in various applications. Single crystalline  $\text{Ag}_2\text{Se}$  nano wires and polycrystalline  $\text{Ag}_2\text{Se}$  tubes [32], nanofiber bundles [33], nano tubes [26], nano crystals [4, 23, 34] were synthesized. Reactive evaporation method yielded  $\text{Ag}_2\text{Se}$  nanocrystals having grain size 650 nm [23]. Though solvothermal method with single precursor yield nano crystals of  $\text{Ag}_2\text{Se}$  with grain size between 25 – 40 nm, the reaction temperature is 250 °C [34] and we are reporting facile room temperature synthesis of nanocrystalline  $\text{Ag}_2\text{Se}$  with grain size of the order 63 nm. This type of morphology will be useful in the surface area dependent application of semiconducting  $\text{Ag}_2\text{Se}$  nano crystals in photo-catalysis and solar cell.

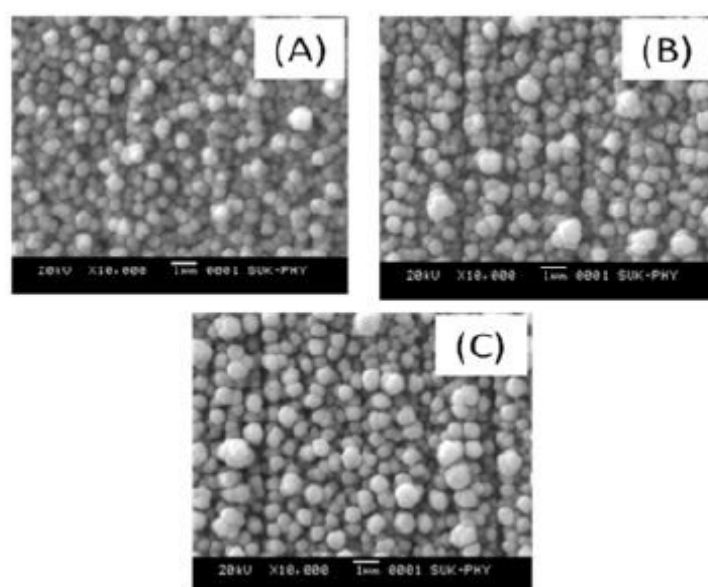


**Fig. 3.** Micrographs of  $\text{Ag}_2\text{Se}$  thin film for different bath concentrations.

**3.5. Optical absorption.** The theory of optical absorption gives the relationship between the absorption coefficients ( $\alpha$ ) and the photon energy ( $h\nu$ ):

$$\alpha = (E_g - h\nu)^n / h\nu, \quad (5)$$

where  $\alpha$  and  $\nu$  are the constants and  $n = 2, 1/2, 3/2, 2, 3$  for direct allowed, direct forbidden, indirect allowed and indirect forbidden transitions respectively. Figure 4 shows the plot of  $(\alpha h\nu)^2$  versus  $h\nu$  of  $\text{Ag}_2\text{Se}$  thin film for samples I, II and III deposited on FTO. The above Eq. (5) gives the band gap ( $E_g$ ) when straight portion of  $(\alpha h\nu)^2$  against  $(h\nu)$  plot is extrapolated to the point  $\alpha = 0$ . It is seen that the plots are linear indicating the mode of transition is of direct nature with the optical band gap ( $E_g$ ) values viz. 1.31, 1.20 and 1.13 eV (Table 2) for concentrations (A), (B) and (C) respectively, which are less than the values reported earlier [4-5] and very close to the standard value of 1.2 eV. The shift in the band gap energy can be attributed to size quantization due to localization of electrons and holes in a confined volume of nanocrystals. Decrease in the band gap is attributed to increase in the size of  $\text{Ag}_2\text{Se}$  crystallites which favors the XRD result i.e. particle size increases with increase in concentration.

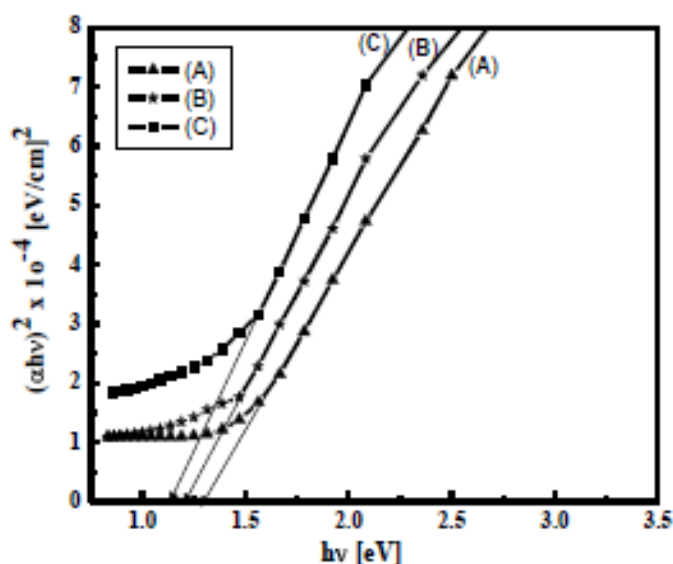


**Fig. 4.** Plot of  $(\alpha h\nu)^2$  versus  $(h\nu)$  of  $\text{Ag}_2\text{Se}$  thin films for different bath concentration.

**3.6. Surface wettability.** The measurement of water contact angle on solid surface, a macroscopic parameter is an empirical diagnostic method for evaluation of thin film property as the chemical and physical processes are dependent on the interaction between solid and liquid. The presence of local inhomogenities, chemical composition and surface morphology in thin film is directly related to the water contact angle of surface [35]. Measurement of surface water contact angle is inversely proportional to the wettability. If the contact angle is less than  $90^\circ$  then water wets the solid showing hydrophilic nature of solid and if it is more than  $90^\circ$  then solid surface is non-wetting called hydrophobic surface of solid. The wettability study of electrodeposited  $\text{Ag}_2\text{Se}$  thin films shows hydrophilic nature of thin films (Fig. 5) contact angle increases from  $58^\circ$  to  $74^\circ$  with increase in bath concentration which is close to that between water and glass ( $72^\circ$ ). Thus it seems that surface of  $\text{Ag}_2\text{Se}$  thin film is highly compact and smooth like surface of glass [36]. The decrease in wettability with increase in concentration is observed due to the increase in particle size with compact arrangement of particles.

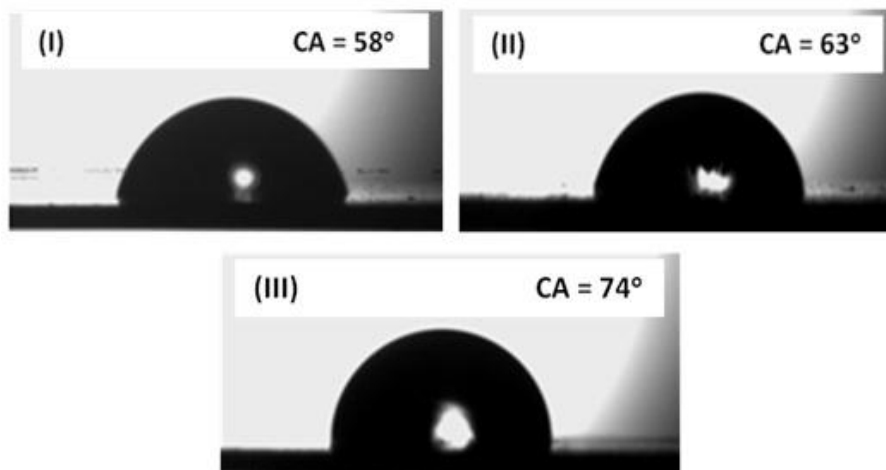


**Fig. 5.** Wettability of  $\text{Ag}_2\text{Se}$  thin films.

Sample (I) for bath concentration A, sample (II) for bath concentration B, sample (III) for bath concentration C.

**3.7. FT-IR.** The spontaneous orientations of dipole moments in semiconductors are carried out by infrared spectroscopy which gives information on atomic arrangement and inter atomic forces in the crystal lattice itself. The FT-IR spectra of  $\text{Ag}_2\text{Se}$  thin film is shown in Fig. 6. The FT-IR absorption bands were found at around wave numbers  $1384.50$  and  $1633.67 \text{ cm}^{-1}$  corresponding to the stretching vibrations of  $\text{Ag} - \text{Se}$  bond which confirms the  $\text{Ag}_2\text{Se}$  formation while the absorption around  $3412 \text{ cm}^{-1}$  is due to free  $-\text{OH}$  group as the samples were synthesized from aqueous electrolytic bath.

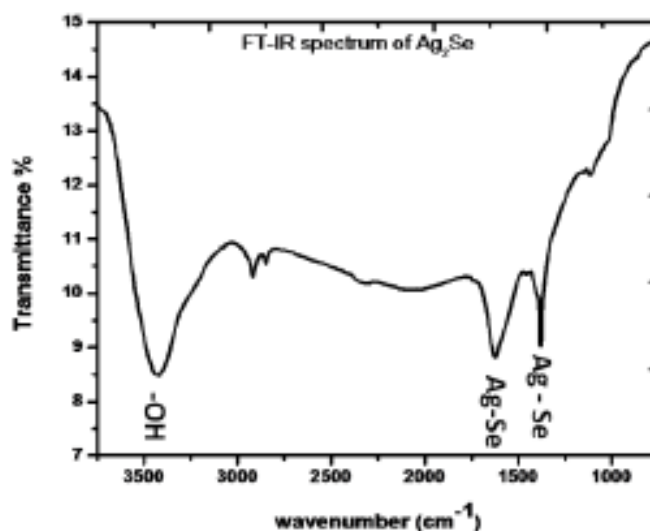


**Fig. 6.** FT-IR spectrum of  $\text{Ag}_2\text{Se}$ .

#### 4. Holographic study

**4.1. Double exposure holographic interferometry (DEHI).** The double exposure holographic interferometry (DEHI) technique is used for thickness and stress measurement of  $\text{Ag}_2\text{Se}$  thin films for different bath concentrations. Figure 7 shows the experimental setup for recording hologram of the thin film.

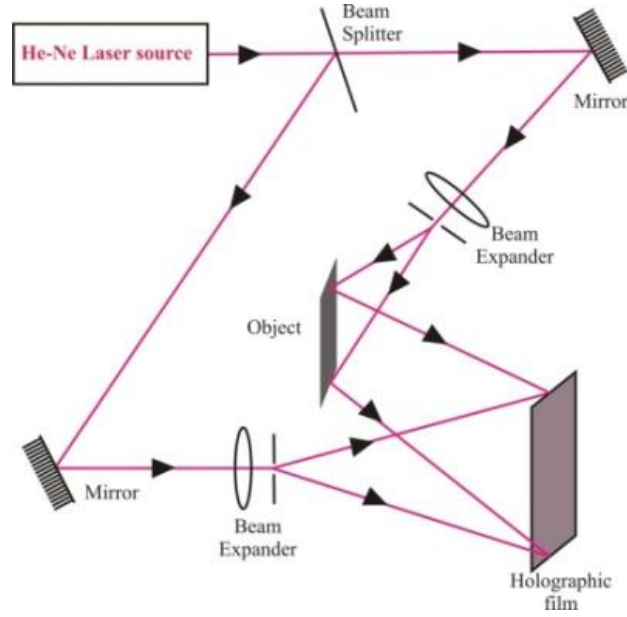


**Fig. 7.** Schematics of experimental setup for hologram recording.

Light from the laser source is passed through beam splitter illuminates the stainless steel substrate. The light scattered from stainless steel substrate carrying the data in terms of wave fronts from stainless steel substrate is taken on holographic plate, which is called as object beam. A part of light (50 %) reflected, incident on another mirror. It is directly incident on holographic film as reference beam. Initially steel substrate was recorded on holographic film as an object without deposition of the film. Secondly the holographic film was exposed by depositing  $\text{Ag}_2\text{Se}$  thin film for few seconds. It is reconstructed as that of the recording position in the path of reference beam, localized fringes are observed on the surface of substrates [37]. While recording the hologram, the substrate is illuminated with a beam of light making an angle ( $\theta_1$ ) with normal and it is viewed at an angle ( $\theta_2$ ) during reconstruction; the reconstructed image has a superimposed fringe pattern corresponding to a displacement of the surface. The displacement in the normal direction is given by

$$d = n\lambda / (\cos\theta_1 + \cos\theta_2), \quad (6)$$

where  $n$  is the total number of fringes,  $\lambda$  is the wavelength of light.

The angles ( $\theta_1$ ) and ( $\theta_2$ ) are sufficiently smaller. Therefore,

$$d = n\lambda/2. \quad (7)$$

After counting relative number of fringes  $n$ , deformation of object surface was calculated, using Eq. (7) [38]. The mass of the film was calculated using the following relation:

$$\text{mass} = \text{density} \times \text{volume}. \quad (8)$$

The stress to substrate is given by the formula [38, 39]:

$$S = (t_s^2 Y_s \Delta) / (3l^2 t_f), \quad (9)$$

where,  $S$  = stress ( $\text{dyne/cm}^2$ ),  $l$  = length of the substrate on which thin film is deposited,  $t_s$  = substrate thickness,  $t_f$  = film thickness,  $Y_s$  = Young's modulus and  $\Delta$  = deflection of the substrate.

The holograms were recorded on holographic plates (Kodak 8E 75 HD) for different

time intervals. The holographic film was processed and replaced only in the reference wave path. The reconstructed image of substrate was observed with the reference beam, which shows the fringes localized on its surface [40, 41]. Using equations (7) – (9), estimated values of thickness, mass and stress of  $\text{Ag}_2\text{Se}$  thin film [38, 39, 42] are given in Table 3.

**4.2. Variation in thickness and mass.** Recorded holograms of  $\text{Ag}_2\text{Se}$  thin films by DEHI for bath concentration (A), (B) and (C) varying deposition time are shown in Fig. 8(a), Fig. 8(b) and Fig. 8(c) respectively. The increase in precursor concentration and deposition time increases the number of localized fringes with increase in thickness of thin film calculated using relation (7) shown in Fig. 9. These fringes are formed due to the interference between the light waves reflected from stainless steel substrate before and after deposition of  $\text{Ag}_2\text{Se}$  thin film. These fringes clearly indicate the deflection of stainless steel substrate due to the deposition of material onto it. Decrease in fringe width is observed with increase in both concentration and deposition time. The deposited mass of  $\text{Ag}_2\text{Se}$  in form of thin films increases with increase in concentration as well as deposition time as shown in Table 3.

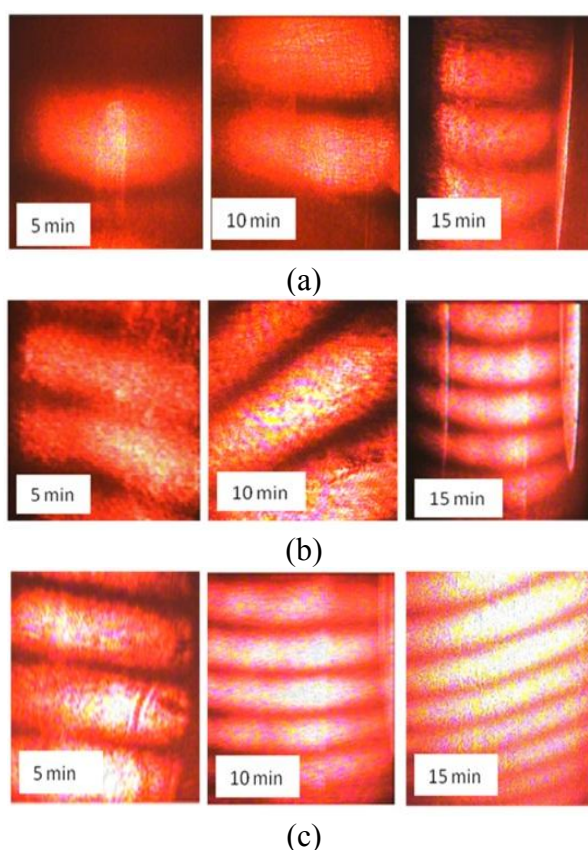


**Fig. 8.** Holograms of  $\text{Ag}_2\text{Se}$  thin films for bath concentration (a) - (A); (b) - (B); (c) - (C).

Thickness of thin film depends on applied voltage and concentration. Nucleation and growth of  $\text{Ag}_2\text{Se}$  in electrolyte increase with increase in concentration and time as well. As the concentration increases the number of cations and anions present in electrolyte accelerates the nucleation and growth processes resulting into higher thickness and more mass deposition for same time interval. Further increase in deposition time beyond 15 minutes, thickness goes on decreasing due to saturation and overgrowth of thin film with less adherence causing rupture and failure of thin film. Increase in the film thickness leads to agglomeration of  $\text{Ag}_2\text{Se}$  nano particles due to Van der Waals interaction between them causing increase in particle size and compactness of thin film revealed by XRD and microstructure respectively which decreases the wettability of  $\text{Ag}_2\text{Se}$  thin film.

**4.3. Stress to substrate.** During deposition of the thin films, an intrinsic stress is generated due to cantilever deflection. Hence, in practice the thin films could not be deposited stress free. It is necessary to leave the stressed deposited layer freestanding which is an important component of the desired device. It is possible by removing the underlying sacrificial layer by increasing the thickness of thin film because the neutral bending line of the cantilever located in the middle changes its location with layer thickness. As a consequence the process induced stress can release and deform the deposited layer. The value of stress to substrate of  $\text{Ag}_2\text{Se}$  thin films was calculated using relation (9) summarized in Table 3. From Fig. 10 it is seen that as thickness (or concentration) of the thin film increases, stress to substrate decreases with increase in particle size.

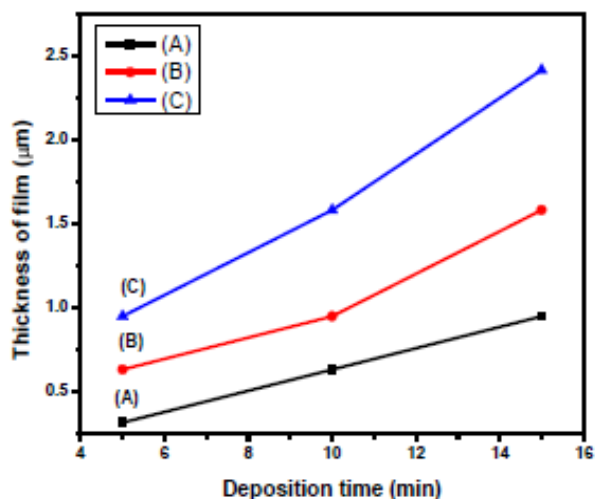


**Fig. 9.** Thickness of deposited thin films for different time and concentrations.

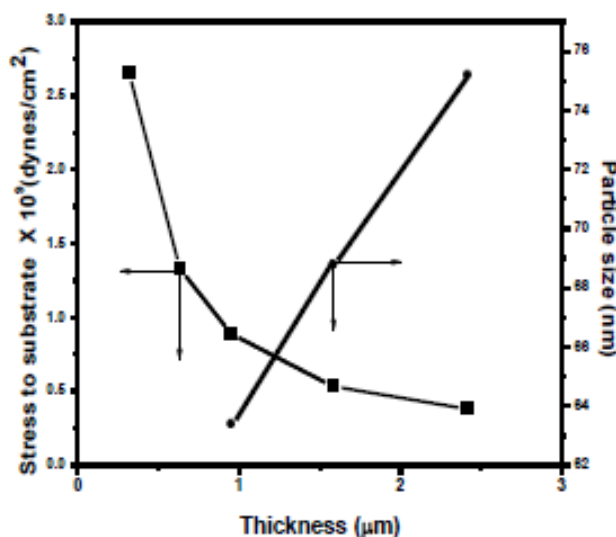


**Fig. 10.** Variation in stress and particle size with thickness of electrodeposited  $\text{Ag}_2\text{Se}$  thin film.

Increase in the concentration of electrolyte accelerates nucleation and growth mechanism resulting into more thickness. Agglomeration of the  $\text{Ag}_2\text{Se}$  particles increases grain size with saturation in Van der Waals interaction with minimization of interfacial energy. Thus unbalanced interaction between particles goes on decreasing which imparts low stress to the substrates. Calculated values of holographic parameters such as no. of fringes, thickness, mass and stress of thin film for bath concentration (A), (B) and (C) are summarized in Table 3.

Table 3. Holographic parameters for Ag<sub>2</sub>Se thin films.

Bath Conc.	Deposition Time, min	No. of Fringes	Thickness, $\mu\text{m}$	Mass deposited, mg	Stress $\times 10^9$ , dyne/cm <sup>2</sup>
A	05	01	0.3164	0.779	2.66
	10	02	0.6328	1.560	1.33
	15	03	0.9492	2.399	0.889
B	05	02	0.6328	1.560	1.330
	10	03	0.9492	2.399	0.889
	15	05	1.582	3.899	0.533
C	05	03	0.9492	2.399	0.889
	10	05	1.582	3.899	0.533
	15	07	2.4148	5.460	0.380

## 5. Conclusions

Nanocrystalline Ag<sub>2</sub>Se thin films have been successfully synthesized from aqueous precursor solution with simple eco- friendly electrodeposition technique at room temperature. Effects on crystallite size, band gap energy and wettability have been studied varying precursor concentration. The double exposure holographic interferometry (DEHI) technique has been successfully employed to explain the effect of concentration on physical properties of thin films by calculating thickness and stress of thin film. From the present study it is clear that nano crystalline silver selenide thin films will be grown at room temperature for various device applications.

## Acknowledgment

Authors are very much grateful to UGC, New Delhi (India) for providing financial support through M.R.P. scheme no. F. No. 36-209/2008(SR).

## References

- [1] P.K. Khanna, B.K. Das // *Mater. Lett.* **58** (2004) 1030.
- [2] P. Boolchand, W.J. Bresser // *Nature* **410** (2001) 1070.
- [3] A. Nunez Rodriguez, M.T.S. Nair, P.K. Nair // *Semiconductor Science Technology* **20** (2005) 576.
- [4] M. C. Santosh Kumar, B. Pradeep // *Bull. Mater. Sci.* **25** (2002) 407.
- [5] M. Ferhat, J. Nagao // *Appl. Phys. Lett.* **88** (2000) 813.
- [6] Z. Vucic, J. Gladic // *J. Cryst. Growth* **205** (1999) 136.
- [7] M. Kobayashi // *Solid State Ionics* **39** (1990) 121.
- [8] B. Gates, Y. Wu, P. Yang, Y. Xia // *J. Am. Chem. Soc.* **123** (2001) 11500.
- [9] M.M. Parish, P.B. Littlewood // *Nature* **426** (2003) 162.
- [10] R. Xu, A. Husmann, T.F. Rosenbaum, M.L. Saboungi, J.E Enderby, P.B Littlewood // *Nature* **390** (1997) 57.
- [11] Gur, N.A. Fromer, M.L. Geier, A.P. Alivisatos // *Science* **310** (2005) 462.
- [12] V.L.Colvin, M.C. Schlamp, A.P. Alivisatos // *Nature* **370** (1994) 354.
- [13] N. Tessler, V. Medvedev, M. Kazes, S. Kan, U. Banin // *Science* **295** (2002) 1506.
- [14] D.L. Klein, R. Roth, A.K.L. Lim, A.P. Alivisatos, P.L. McEuen // *Nature* **389** (1997) 699.

- [15] D.V. Talapin, C.B. Murray // *Science* **310** (2005) 86.
- [16] W.C.W. Chan, S. Nie // *Science* **281** (1998) 2016.
- [17] V. Damodara Das, D. Karunakaran // *J. Appl. Phys.* **68** (1990) 2105.
- [18] C.D. Lokhande, K.M. Gadave // *Mater. Chem. Phys.* **36** (1993) 119.
- [19] A.B. Kulkarni, M.D. Uplane, C.D. Lokhande // *Thin Solid Films* **260** (1995) 14.
- [20] B. Pejova, M. Najdoski, I. Grozdanov, S.K. Dey // *Mater. Lett.* **43** (2000) 269.
- [21] Y.J. Glanville, D.G. Narehood, P.E. Sokol, A. Amma, T. Mallouk // *J. Mater. Chem.* **12** (2002) 2433.
- [22] S.J. Pawar, P.P. Chikode, V.J. Fulari, M.B. Dongare // *Mater. Sci. Eng. B* **37** (2007) 232.
- [23] H. Cao, Y. Xiao, Y. Lu, J. Yin, B. Li, S. Wu, X. Wu // *Nano Res.* **3** (12) (2010) 863.
- [24] A. Sahu, L. Qi, M. S. Kang, D. Deng, D.J. Norris // *J. Am. Chem. Soc.* **133** (2011) 6509.
- [25] P. T. Kissinger, W. R. Heineman // *J. of Chem. Edu.* **60** (1983) 702.
- [26] S. Zhang, C. Fang, W. Wei, B. Jin, Y. Tian, Y. Shen, J. Yang, H. Gao // *J. Phys. Chem. C* **111** (2007) 4168.
- [27] C. Ruizhi, X. Dongsheng, G. Guolin, T. Youqi // *J. of Mater. Chem.* **12** (2002) 1437.
- [28] L.V. Azároff, R. Kaplow, N. Kato, R.J. Weiss, A.J.C. Wilson, R.A. Young, *X-ray Diffraction* (McGraw-Hill, New York, 1974).
- [29] JCPDS card No. 24-1041
- [30] B.D. Cullity, *Elements of X-rays Diffraction* (Addison-Wesley, London, 1978).
- [31] C.M. Jiao; Z.Z. Wang, Z. Ye, Y. Hu, W.C. Fan // *J. Fire Sci.* **24** (2006) 47.
- [32] D.T. Schoen, C. Xie, Y. Cui // *J. Am. Chem. Soc.* **129** (2007)
- [33] H. Wang, L. Qi // *Adv. Funct. Mater.* **18** (2008) 1249.
- [34] S.K. Batabyal, C. Basu, A.R. Das, G.S. Sanyal // *Crystal Growth & Design* **4** (2004) 509.
- [35] F. Xia, H. Ge, Y. Hou, T. Sun, L. Chen, G. Zhang, L. Jiang // *Adv. Mater.* **19** (2007) 2520.
- [36] R.S. Mane, H.Y. Hee, C.D. Lokhande, S.D. Sartale, S.H. Han // *Appl. Surf. Sci.* **246** (2005) 271.
- [37] G.W. Stroke, *An introduction of coherent optics and holography* (Academic Press, New York, 1969).
- [38] V.B. Prabhune, V.J. Fulari // *Opt. Commun.* **282** (2009) 2118.
- [39] V.J. Fulari, V.P. Malekar, S.A. Gangawane // *Progress in Electromagnetic Research C* **12** (2010) 53.
- [40] I.A. Lyavshuk, A.M. Lyalikov // *Quantum electron.* **36** (2006)154.
- [41] A.M. Lyalikov // *Opt. Spekr.* **93** (2002) 512.
- [42] G.A. Korn, T.M. Korn, *Mathematical Handbook for Scientists and Engineers* (McGraw-Hill, New York, 1961).